[Geophysical Research Letters]

Supporting Information for

Barium Isotopes Indicate Spatiotemporal Heterogeneity of Marine Primary Productivity during the Toarcian Oceanic Anoxic Event

Wenhan Chen[1,2], David B. Kemp[3*], Hugh C. Jenkyns[4], Stuart A. Robinson[4], Yibo Lin[5], Jun Hu[1,2], Zhong Han[6], Tianchen He[7], Feifei Zhang[5], Xilei Sun[3], Guangyu Shi[8], Chao Li[1,2*]

[1]State Key Laboratory of Oil and Gas Reservoir Geology and Exploitation & Institute of Sedimentary Geology, Chengdu University of Technology, Chengdu 610059, China

[2]International Center for Sedimentary Geochemistry and Biogeochemistry Research, Chengdu University of Technology, Chengdu 610059, China

[3]State Key Laboratory of Geomicrobiology and Environmental Changes and Hubei Key Laboratory of Critical Zone Evolution, School of Earth and Planetary Sciences, China University of Geosciences, Wuhan 430074, China

[4]Department of Earth Sciences, University of Oxford, Oxford OX1 3AN, UK

[5]School of Earth Sciences and Engineering, Nanjing University, Nanjing 210023, China

[6]State Key Laboratory of Palaeobiology and Stratigraphy, Nanjing Institute of Geology and Palaeontology, Chinese Academy of Sciences, Nanjing 210008, China

[7]College of Oceanography, Hohai University, Nanjing 210024, China

[8]Wuhan SampleSolution Analytical Technology Co., Ltd, Wuhan 430075, China

* Corresponding authors: David B. Kemp (davidkemp@cug.edu.cn); Chao Li (chaoli@cdut.edu.cn)

Contents of this file

Additional Supporting Information (Files uploaded separately)

Text S1. Reliability of traditional productivity proxies

A variety of traditional geochemical proxies have been employed to reconstruct marine primary productivity during the T-OAE, but they may have interpretative limitations. For example, bulk sedimentary phosphorus (P), applied in both NW Tethys (Bodin et al., 2010) and SE Panthalassa (Fantasia et al., 2018), was likely prone to substantial detrital P contributions that undermine its fidelity as a local productivity indicator (Algeo and Ingall, 2007). Multiple nitrogen-isotope records from the European Epicontinental Shelf and northern Gondwana margin (Ruebsam et al., 2020 and references therein) might also be compromised, as they can be altered by laboratory decalcification (Schlachter and Connolly, 2014). Furthermore, the ratio of Ba/Rb has been used to infer excess biogenic barite accumulation and hence surface productivity in the Belluno Trough, NW Tethys (Bellanca et al., 1999). However, barite preservation is strongly redox-dependent, and the particulates would be largely dissolved under euxinic conditions, reducing its utility to trace marine primary productivity (Schoepfer et al., 2015). Taken together, an alternative, more reliable proxy is needed to resolve the changes in marine productivity during the T-OAE.

Text S2. Geological setting

Nianduo section, Tethys Himalaya

The studied Nianduo section (Nyalam area, Tibet, southern China) was deposited on the Kioto carbonate platform, Tethys Himalaya (28.6811° N, 86.1353° E; Fig. 1B). Commonly observed sedimentary structures at Nianduo, such as hummocky and swaley cross-bedding, gutter casts, and ripple marks, suggest a dynamic shallow-water environment above storm wave base, with an inferred paleo-depth of tens of meters during the T-OAE (Han et al., 2016, 2018). The upper Lower to lower Middle Jurassic marine succession, constituting sedimentary remnants representative of the northern margin of the Indian continent, has been subdivided into two stratigraphic units: the Pupuga and Nieniexiongla Formations (Wang et al., 1980). The Pupuga Formation was deposited on a shallow-water carbonate platform, consisting mainly of the thick-bedded grainstones/packstones deposited under turbulent-water conditions, intercalated with sandstones and mudstones. The overlying Nieniexiongla Formation was deposited in a relatively deeper water ramp environment, characterized by thin-bedded marls in the lower part and more abundant siltstones in the upper part.

In the Nianduo section, the occurrence of *Lithiotis* bivalves in the upper Pupuga Formation suggests an interval of late Pliensbachian to early Toarcian age (Jadoul et al., 1998). In the overlying lower Nieniexiongla Formation, ammonites from nearby sections, such as *Polyplectus discoides*, *Dumortieria sp.*, and *Phymatoceras* cf. *crasstcosta*, indicate the *bifrons–levesquei* Zones of the middle–upper Toarcian (Yin, 2010). The Pupuga–Nieniexiongla boundary marks the T-OAE onset due to the identification of a N-CIE of 2.5‰ spanning a thickness of around 28 m (Han et al., 2018; Fig. 2A).

Dogna core, Belluno Trough Basin

The Belluno Trough Basin (southern Alps, northern Italy) was a relatively deep (1,500–2,000 m in depth), narrow, and elongated basin (Fig. 1C), resembling the modern-day “Tongue of the Ocean” that dissects the Bahama Banks (Bosellini et al., 1981; Picotti and Cobianchi, 2017). The basin was located on the continental margin of the Apulian Plate in the Alpine-Mediterranean Tethys (Bosellini et al., 1981; Winterer and Bosellini, 1981). The formerly extensive carbonate-platform belt disintegrated during the Early Jurassic due to active rifting and the opening of the

Central North Atlantic Ocean, with a distinct "horst-and-graben" structure formed in a pelagic setting (Bosellini et al., 1981; Winterer and Bosellini, 1981; Masetti et al., 2012). During the Early Jurassic, the Belluno Trough Basin was bounded by the Trento Platform/Plateau to the west and the Friuli Platform to the east (Fig. 1C), with the Igne Formation spanning the Toarcian–Aalenian interval and comprising variably clay-rich calcareous facies rich in pelagic bivalves, radiolaria, and echinoderm fragments (Bosellini et al., 1981; Jenkyns, 1988; Picotti and Cobianchi, 2017).

The rocks of the studied Dogna core (46.4479° N, 13.3150° E) were deposited in the Belluno Trough Basin, with an estimated paleo-depth of >1,000 m (Bosellini et al., 1981). The material in the Dogna core is characterized by interbedded limestone, marlstone, and calcareous shale. The pelagic setting is supported by commonly observed calcareous nannofossils (e.g., coccolithophorids and *Schizosphaerella punctulata*) in marlstone and limestone in the nearby Longarone section (Bellanca et al., 1999), though there was also a potential background supply of fine-grained material from the neighboring carbonate platform (Trento) (Bosellini et al., 1981). In stratigraphically equivalent sections nearby, the occurrence of *Dactylioceras* cf. *anguiforme* 60 cm above the top of the diagnostic carbonate-shale sequence indicates the upper *falciferum* Zone. Multiple *Hildoceras* species at a stratigraphically higher level indicate the *bifrons* Zone. Thus, the alternating carbonate-shale sediments in the Dogna core were assigned to the lower *falciferum* Zone (Jenkyns et al., 1985). On this biostratigraphic basis, the N-CIEs (spanning a thickness of around 18 m) identified in both organic and inorganic carbon archives in the Dogna core unambiguously constrain the T-OAE chemostratigraphically (Jenkyns et al., 2001; Fig. 2B).

Text S3. Details of analytical protocols

Carbonate-hosted major and trace elements

To minimize the potential alteration of the primary Ba-isotope signals by organic-rich material in the bulk carbonate rocks via cation absorption, a sequential leaching method was followed (Lin et al., 2020). In detail, around 200 mg of powdered sample was first rinsed with Milli-Q water to remove any water-soluble phases. The residue was then rinsed with 1 M ammonium acetate to remove the Ba adsorbed on the surfaces of organic matter and carbonate minerals. Finally, the residue was rinsed with Milli-Q water before extracting the Ba fraction from the lattices of carbonate minerals with 1 M acetic acid (Lin et al., 2020). After leaching and centrifuging, the supernatant was separated and dried down on a hotplate at 120 °C. The leachate was then dissolved and stored in 6 M HCl for elemental and isotopic analyses. An aliquot of each solution was taken out, dried down, and redissolved in 3% HNO_3 for the measurement of major and trace elements through a Thermo iCAP Pro ICP-OES and a Thermo Element XR HR-ICP-MS, respectively, at Nanjing University. Accuracy was monitored by analyzing the limestone reference materials JLs-1 and GSR-13. JLs-1, from the Geological Survey of Japan, is a dark grey limestone collected from Kamiisocho, Hokkaido, with a Ba concentration of 476 µg/g. GSR-13 is from the China National Research Centre of Geoanalysis, and is a grey-white limestone collected from Xishan, Beijing, with a Ba concentration of 10 µg/g. Analytical reproducibility of samples yielded relative standard deviations (RSDs) for all elements of <5% (1SD).

Carbonate barium isotopes ($\delta^{138}Ba_{carb}$)

An aliquot of each solution containing 200 ng of Ba was taken out from the stock solution and mixed with ^{130}Ba–^{135}Ba double spikes at a sample/spike ratio of 4:1 (Lin et al., 2020).

Subsequently, the spike-sample mixtures were dried down and redissolved in 2.5 M HCl, followed by the Ba purification protocols detailed in Lin et al. (2020). Specifically, 1 mL of AG 50 W-X8 cation exchange resin loaded to a 10 mL cation column was at first rinsed with 10 mL of 1 M HF, 7 mL of 6 M HCl, and 10 mL of Milli-Q water before being preconditioned with 1 mL of 2.5 M HCl. The sample was then loaded onto the column in 1 mL of 2.5 M HCl. An additional 3 mL and 5.5 mL of 2.5 M HCl and 6.5 mL of 1.7 M HNO_3 were added to the column in sequence to separate Ba from the matrix elements, in particular from the REEs, through elution.

The collected solution containing purified Ba was dried down and dissolved into approximately 100-ppb solutions with 3% HNO_3 for the measurement of $\delta^{138}Ba_{carb}$ using a Thermo Neptune XT MC-ICP-MS at Nanjing University. The $\delta^{138}Ba$ values of standards SRM 3104a and JLs-1 were determined bracketing every five samples in measuring sessions to monitor the measurement accuracy. The measured $\delta^{138}Ba$ values of SRM 3104a and JLs-1 are 0.00 ± 0.04‰ (2SD, n = 11) and 0.03 ± 0.02‰ (2SD, n = 9), respectively. The JLs-1 value represents three independent digestions processed through the full chemical purification procedure, with each digest measured in triplicate by MC-ICP-MS. Ba concentrations from total procedural blanks were <1 ng, much lower than the Ba concentrations (~200 ng) separated from the bulk samples.

Fe-speciation

Fe-speciation analyses were performed on the Dogna samples following refined extraction protocols (Jin et al., 2016) at the State Key Laboratory of Biogeology and Environmental Geology, China University of Geosciences (Wuhan). Around 0.1 g of powdered sample was reacted with a 10-mL solution of 1 M sodium acetate and acetic acid at 50 °C for 48 h to extract iron in carbonates (Fe_{CARB}). The residue was then mixed with a 10-mL solution of sodium dithionite and sodium citrate for 2 h to dissolve Fe (oxyhydr)oxides (Fe_{OX}). Subsequently, the mixed ferrous–ferric minerals (Fe_{MAG}) were extracted by adding 10 mL of ammonium oxalate for 6 h. The chromium reduction technique was followed to determine the fraction of Fe sulfides (Fe_{PY}) on separate splits of each sample (Canfield et al., 1986). The sample powders (1–2 g) were treated with 40 mL of 1 M reduced chromium chloride ($CrCl_2$) solution and 20 mL of 6 M HCl for 1 h. The produced H_2S was then purged under a nitrogen atmosphere (N_2) and trapped as Ag_2S by bubbling through an $AgNO_3$ solution (0.1 M). Subsequently, the precipitated Ag_2S was filtered and dried down for the determination of sulfide in the sample by gravimetry. The amount of Fe_{PY} in the original sample was then calculated stoichiometrically. The iron concentration of each sequential extract was obtained via a ThermoFisher iCE 3300 atomic absorption spectrometer (AAS). Replicate extractions of samples and reference material WHIT (a Lower Jurassic fine-grained, laminated, organic carbon-rich mudstone deposited in an anoxic water column) yielded RSDs of <5% for all highly reactive Fe phases.

Separate splits of each sample were used for the measurement of total Fe concentrations (Fe_{tot}) at ALS Minerals, Guangzhou. In detail, 0.1 g of powdered sample was mixed with sodium peroxide flux (1.1 g) and then fused in a 700 °C furnace. The resulting melt was cooled and dissolved in 30% hydrochloric acid. This solution was then analyzed for Fe_{tot} via an inductively coupled plasma-atomic emission spectrometry (ICP-AES). Accuracy was monitored by analyzing reference materials GBW07281 and GBW07170. Repeated measurement of samples yielded RSDs of <5%.

P-speciation and whole-rock major elements

Before utilizing the P-phase partitioning approach, we used the melting method on the

Dogna samples (n = 28) to obtain the whole-rock major-element concentrations, such as total P (P_{tot}), at Wuhan SampleSolution Analytical Technology Co., Ltd. In detail, around 0.6 g of powdered sample was weighed out and then melted at 1050 °C for 15 min. The flux is a mixture of lithium tetraborate, lithium metaborate, and lithium fluoride (45:10:5). Ammonium nitrate and lithium bromide were used as oxidants and release agents, respectively. Zsx Primus II wavelength dispersive X-ray fluorescence spectrometer (XRF) produced by RIGAKU, Japan, was used for the analysis of major elements in the whole rock. The standard curve was established using the national standard material: rock standard sample GBW07101-14, soil standard sample GBW07401-08, and stream sediment standard sample GBW07302-12. The data were corrected by the theoretical α coefficient method. Repeated measurement of samples yielded RSDs of <2%.

P-phase partitioning analyses were performed on the same batch of samples (n = 28) using a revised sequential extraction method (Thompson et al., 2019) at the State Key Laboratory of Biogeology and Environmental Geology, China University of Geosciences (Wuhan). Around 0.15 g of powdered sample was used for the sequential P extraction. In detail, the sample powder was treated with a sodium dithionite solution (buffered with bicarbonate to pH 7.6) for 8 h at room temperature to extract poorly crystalline Fe (oxyhydr)oxides (P_{Fe1}); Authigenic P (P_{auth}; which targets carbonate fluorapatite) was extracted using a sodium acetate solution at pH 4 for 6 h at room temperature; Detrital apatite (P_{det}) was extracted using a 10% HCl solution for 16 h at room temperature; P_{mag} (which targets P associated with magnetite) was extracted using an ammonium oxalate solution for 6 h at room temperature. P_{Fe2} (i.e., more crystalline Fe (oxyhydr)oxide minerals) was extracted using a sodium dithionite solution (buffered with citrate to pH 4.8) for 6 h at room temperature. The residue was ashed (550 °C for 2 h) and reacted with 10% HCl solution for 16 h at room temperature to liberate organic-bound P (P_{org}). Fe (oxyhydr)oxide-bound P (P_{Fe}) is defined as the sum of $P_{Fe1} + P_{Fe2} + P_{mag}$. The P content of the various extracts was determined either by using the molybdate blue method (Ruttenberg, 1992) at a wavelength of 880 nm or by inductively coupled plasma optical emission spectrometry (ICP-OES) for solutions where the matrix interferes with the molybdate blue method (P_{Fe1}, P_{Fe2}, and P_{mag}). Replicate analyses of in-house reference materials (n = 5) yielded an RSD of <10% for each step, except for P_{Fe}, where the low concentrations resulted in an RSD of <20%.

Hg concentration

Hg concentration was measured using a Milestone DMA-80 Evo at the School of Earth Sciences, China University of Geosciences (Wuhan). Around 100 mg of powdered sample was weighed out and then heated to 1000 °C under an oxygen flow to be thermally decomposed. Mercury species were then catalyzed to be reduced and trapped on a gold amalgamator, followed by subsequent release and measurement. A soil Reference Standard (GBW07423, 32 ± 3 ng/g Hg) was analyzed after every ten samples to monitor accuracy. Analytical precision based on these standards was better than ± 2.44 ng/g (2SD).

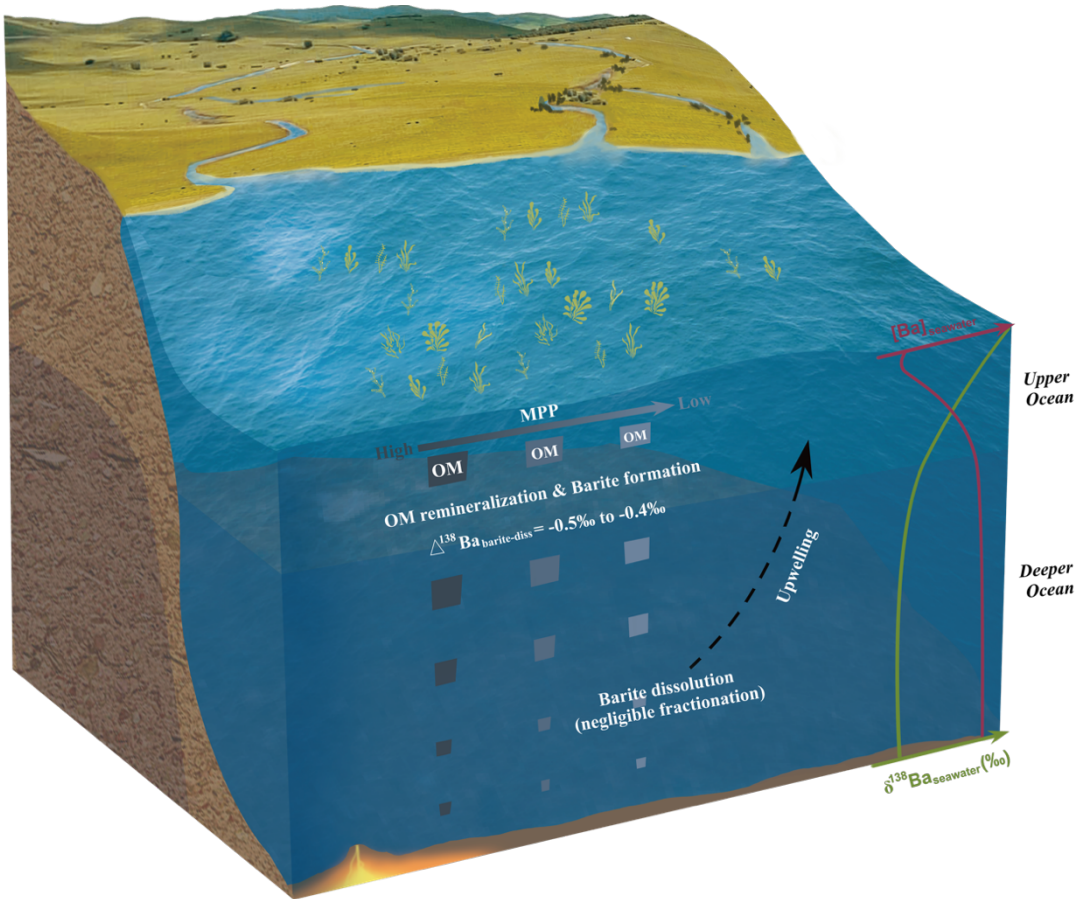

Figure S1. A schematic diagram illustrating marine Ba cycling. The lower right panel denotes simplified profiles of dissolved Ba concentrations (rose red) and δ^{138}Ba (olive green) from the northeast Pacific Ocean at the SAFe site (Geyman et al., 2019), showing a distinct quasi-nutrient type distribution. MPP, marine primary productivity; OM, organic matter; $\Delta^{138}Ba_{barite–diss}$ = $\delta^{138}Ba_{barite}$–$\delta^{138}Ba_{diss}$.

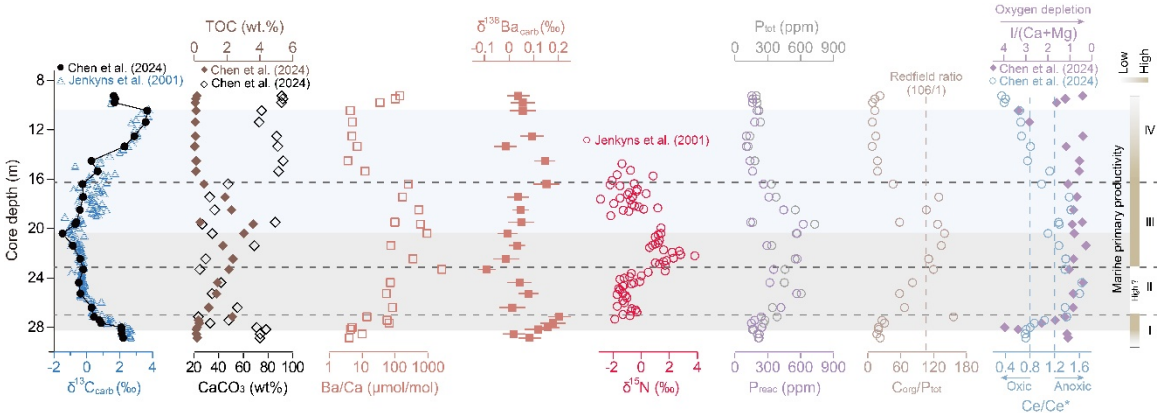

Figure S2. Supplementary geochemical data from the Dogna core in the Lower Toarcian. $CaCO_3$, I/(Ca+Mg), and Ce/Ce* data are from Chen et al. (2024). $\delta^{15}N$ data are from Jenkyns et al. (2001).

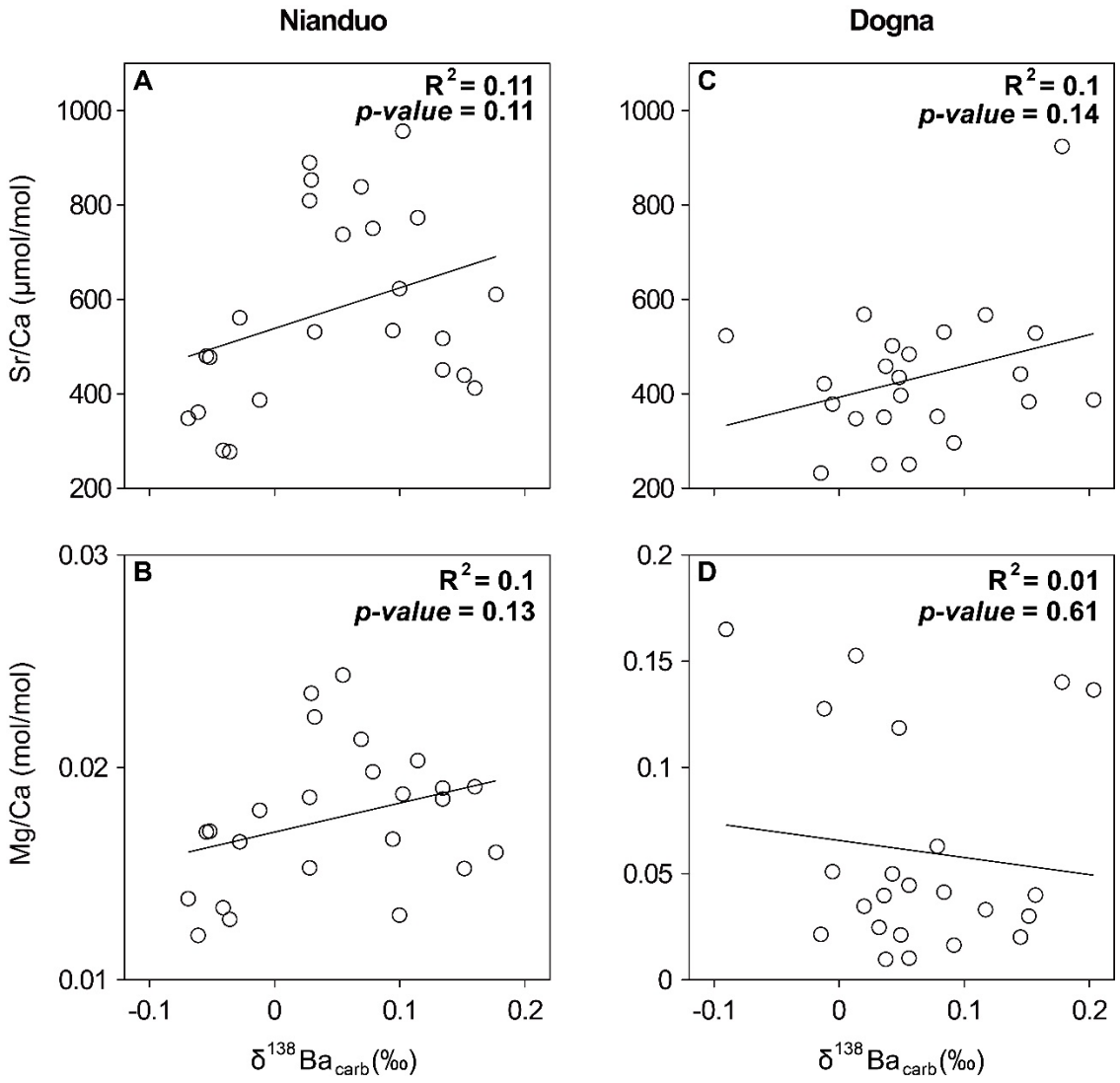

Figure S3. Cross-plots of $\delta^{138}Ba_{carb}$ *versus* molar ratios of Sr/Ca and Mg/Ca from the Nianduo section (panels A and B) and Dogna core (panels C and D).

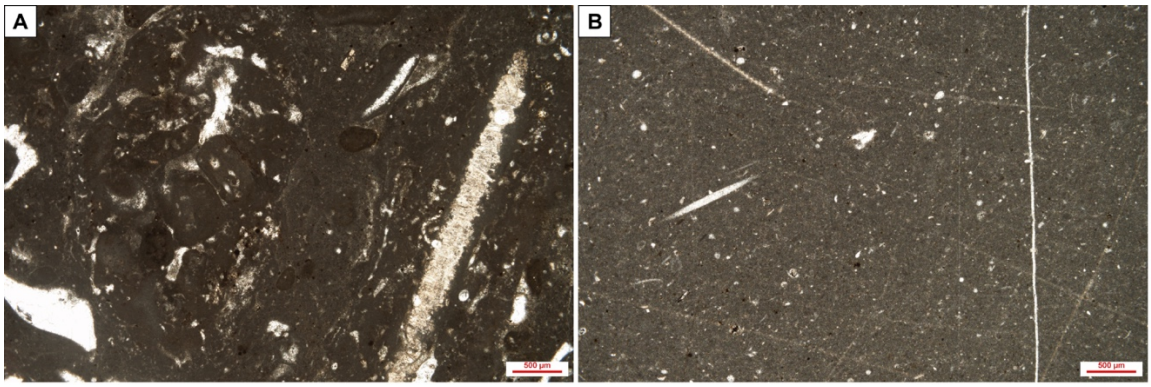

Figure S4. Photomicrographs of characteristic microfacies of our analyzed samples in the Nianduo section. Panel A (–1.6 m section height, Pupuga Formation) showing bioclastic wackestones prior to the T-OAE N-CIE. Panel B (2.4 m section height, Nieniexiongla Formation) showing micrite during the T-OAE N-CIE interval.

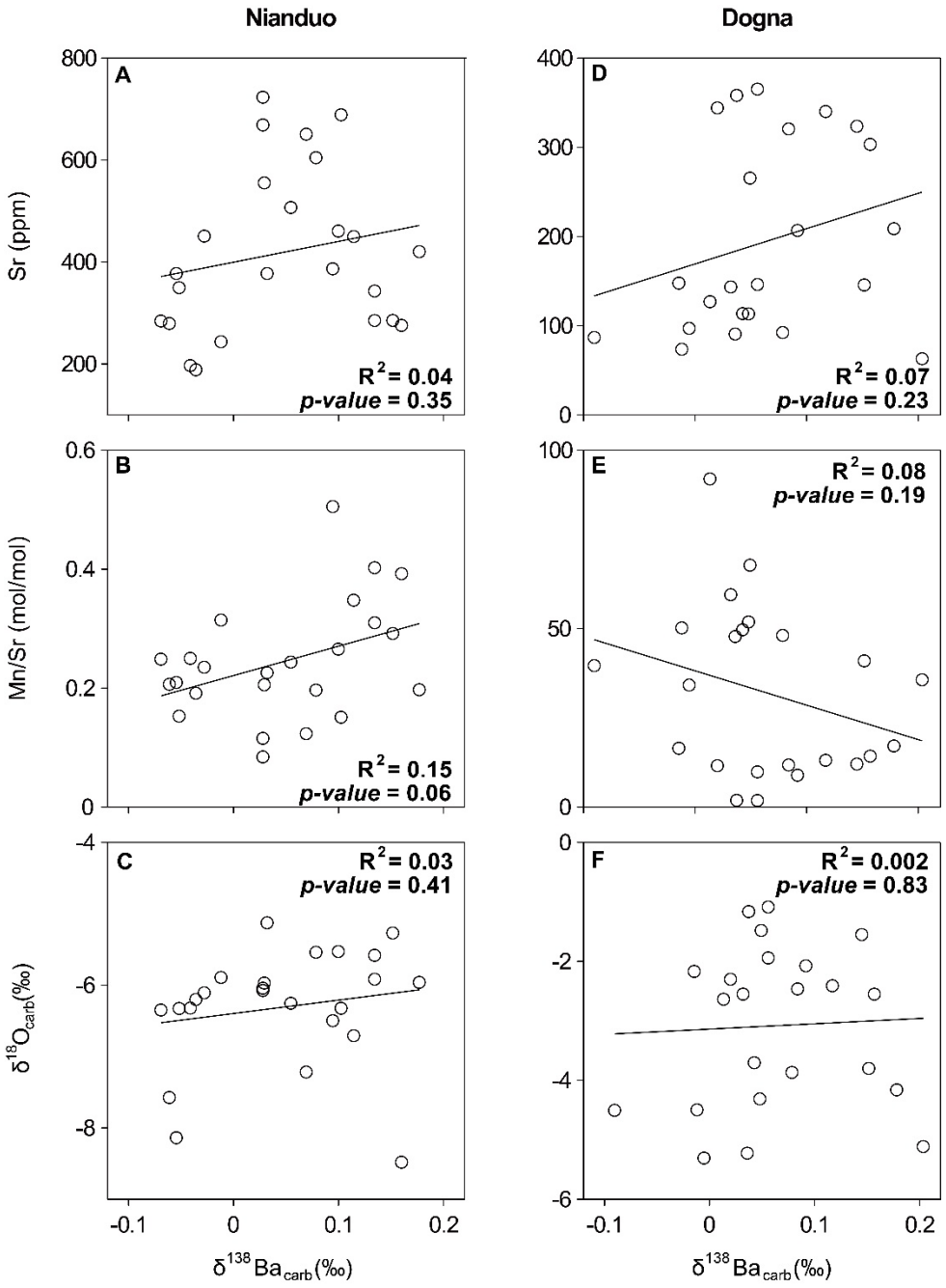

Figure S5. Cross-plots of $\delta^{138}Ba_{carb}$ *versus* Sr concentration, Mn/Sr molar ratio, and $\delta^{18}O_{carb}$ from the Nianduo section (panels A–C) and Dogna core (panels D–F). Note $\delta^{18}O_{carb}$ data at Nianduo and Dogna are from Han et al. (2018) and Chen et al. (2024), respectively.

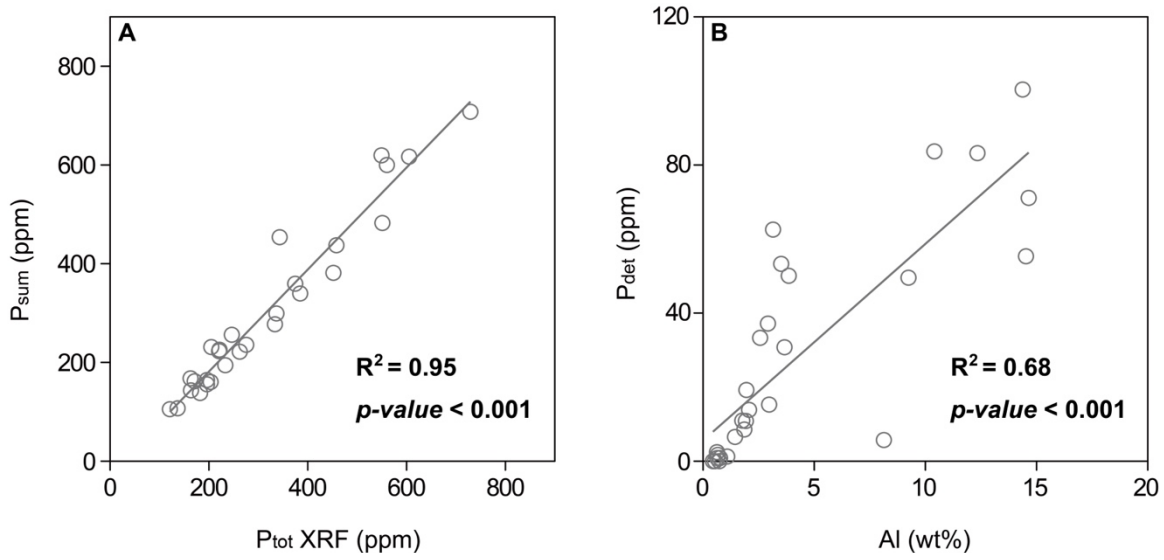

Figure S6. (A) Assessment of phosphorus extraction proficiency based on the correlation between P_{tot} (as determined from XRF) and the sum of each P extract (P_{sum}) following the sequential extraction. (B) The relationship between Al and P_{det} concentrations.

(A) Nianduo section: d18Ocarb data are from Han et al. (2018); https://doi.org/10.1016/j.epsl.2018.02.017

Height (m)	d18Ocarb	d138Ba	2SD	Ba/Ca (μ mol/mol)	Al/Ca (mol/mol)	Mg/Ca (mol/mol)	Sr/Ca (μ mol/mol)	Mn/Sr (mol/mol)	Sr (ppm)	Al (ppm)
33.4	-6.25	0.05	0.054	2.24	0.0002	0.024	738	0.244	507	39.1
31.4	-6.08	0.03	0.038	2.63	0.0001	0.019	890	0.115	723	26.6
29.4	-6.32	0.10	0.042	3.62	0.0005	0.019	956	0.151	689	111
26.4	-5.97	0.03	0.056	2.84	0.0002	0.023	853	0.205	555	46.4
24.4	-5.54	0.08	0.045	4.13	0.0002	0.020	750	0.197	604	37.6
23.4	-6.71	0.11	0.045	2.86	0.0004	0.020	773	0.348	450	70.6
20.4	-7.22	0.07	0.035	2.97	0.0002	0.021	839	0.123	651	51.0
17.4	-6.11	-0.03	0.033	2.77	0.0002	0.017	561	0.235	451	42.9
12.4	-6.04	0.03	0.051	2.41	0.0002	0.015	809	0.084	669	40.2
9.4	-5.27	0.15	0.055	2.99	0.0019	0.015	439	0.292	285	386
8.4	-5.96	0.18	0.047	4.86	0.0002	0.016	611	0.197	420	39.0
7.8	-5.92	0.13	0.051	5.59	0.0044	0.019	451	0.402	285	858
7.6	-8.48	0.16	0.044	1.72	0.0002	0.019	412	0.392	276	34.6
6.6	-5.53	0.10	0.052	2.37	0.0002	0.013	623	0.265	461	55.1
5.4	-5.13	0.03	0.044	2.73	0.0001	0.022	531	0.226	377	16.8
4.6	-5.58	0.13	0.042	3.86	0.0020	0.019	517	0.310	343	418
3.4	-6.50	0.09	0.051	2.93	0.0003	0.017	534	0.505	387	70.0
2.4	-8.14	-0.05	0.048	3.01	0.0001	0.017	480	0.209	377	22.6
1.4	-6.33	-0.05	0.046	4.29	0.0001	0.017	477	0.153	350	21.5
0.4	-5.89	-0.01	0.047	2.14	0.0001	0.018	387	0.314	244	28.6
-1.6	-6.35	-0.07	0.044	1.41	0.0001	0.014	348	0.249	284	26.7
-2.93	-6.20	-0.04	0.046	1.41	0.0004	0.013	277	0.191	188	76.4
-4.59	-6.32	-0.04	0.056	1.35	0.0001	0.013	280	0.250	197	12.9
-5.6	-7.57	-0.06	0.055	2.78	0.0001	0.012	361	0.206	279	17.4

(B) Dogna core: d18Ocarb, CaCO3, and TOC data are from Chen et al. (2024); https://doi.org/10.1016/j.gloplacha.2024.104631

Core depth (m)	d18Ocarb	CaCO3 (wt%)	TOC (wt%)	OC_corr (wt%)	d138Ba	2SD	Ba/Ca (μ mol/mol)	Al/Ca (mol/mol)	Mg/Ca (mol/mol)	Sr/Ca (μ mol/mol)	Mn/Sr (mol/mol)	Sr (ppm)	Al (ppm)	Fetot (wt.%)	Fecarb (wt.%)	Feox (wt.%)
28.86	-2.46	73.29	0.19	0.72	0.08	0.045	4.02	0.003	0.041	531	11.8	320	481	0.830	0.102	0.051
28.54	-2.30	73.59	0.13	0.50	0.02	0.045	9.92	0.003	0.035	568	11.6	344	622			
28.17	-2.41	78.37	0.13	0.60	0.12	0.055	4.38	0.002	0.033	567	13.1	340	347			
28.01	-2.55	70.72	0.18	0.63	0.16	0.047	4.90	0.004	0.040	529	14.3	303	654			
27.66	-4.16	33.04	0.31	0.46	0.18	0.052	65.8	0.007	0.140	924	17.1	209	457			
27.43	-3.56	48.10	0.28	0.53			56.9	0.003	0.076	826	19.9	294	359	2.02	0.141	0.031
27.15	-5.11	23.50	2.33	3.04	0.20	0.046	13.9	0.014	0.137	387	35.7	63.0	719			
26.4	-2.64	55.16	0.89	1.98	0.01	0.053	82.7	0.013	0.153	347	91.9	127	1411	1.48	0.133	0.034
25.27	-3.87	34.67	1.36	2.08	0.08	0.041	54.0	0.009	0.063	352	48.1	92.3	744			
24.38	-3.70	41.86	1.43	2.46	0.04	0.049	71.9	0.005	0.050	502	49.7	114	315	1.92	0.108	0.020
23.31	-4.50	24.60	2.13	2.82	-0.09	0.036	2627	0.023	0.165	523	39.6	86.8	1159	2.70	0.191	0.068
22.46	-4.50	29.47	2.36	3.35	-0.01	0.053	349	0.024	0.128	421	50.2	73.5	1313	2.50	0.147	0.076
21.38	-2.55	68.86	1.75	5.61	0.03	0.033	74.2	0.002	0.025	251	59.5	143	358	0.789	0.097	0.146
20.4	-5.31	34.76	3.03	4.65	-0.01	0.041	935	0.013	0.051	378	34.2	97.0	1008	2.20	0.316	0.066
19.65	-5.30	26.49	3.59	4.89			586	0.014	0.085	510	26.0	95.4	829			
19.49	-1.48	85.91	0.37	2.61	0.05	0.053	98.1	0.001	0.021	397	67.8	265	268			
18.49	-4.31	36.62	2.28	3.59	0.05	0.033	524	0.007	0.119	435	51.9	113	545	2.00	0.217	0.389
17.45	-5.23	32.68	1.88	2.79	0.04	0.045	168	0.008	0.040	350	47.8	90.7	659			
16.4	-3.80	47.54	0.60	1.14	0.15	0.054	250	0.003	0.030	383	41.0	146	335	2.00	0.099	0.438
15.36	-1.56	88.49	0.11	0.97			12.2	0.001	0.020	372	65.8	258	234	0.600	0.073	0.133
14.52	-1.55	92.31	0.12	1.60	0.14	0.043	3.67	0.001	0.020	442	12.0	324	124			
13.35	-2.17	87.89	0.04	0.31	-0.01	0.047	7.05	0.001	0.021	232	16.5	148	277			
12.52	-2.07	87.02	0.08	0.59	0.09	0.048	4.85	0.001	0.016	296	8.92	207	207			
11.38	-2.01	72.85	0.07	0.27			5.01	0.002	0.037	253	10.0	144	310	1.10	0.085	0.413
10.45	-1.94	74.72	0.11	0.43	0.06	0.052	4.34	0.003	0.045	251	9.86	146	558	0.904	0.091	0.284
9.8	-1.09	90.88	0.07	0.74	0.06	0.049	34.8	0	0.010	484	1.83	365	112	0.700	0.144	0.063
9.5	-1.30	91.93	0.10	1.21			102	0.002	0.011	441	2.33	335	367			
9.25	-1.16	91.23	0.17	1.90	0.04	0.046	140	0.001	0.010	458	1.87	358	350	0.526	0.157	0.064

Femag (wt.%)	Fepy (wt.%)	FeHR (wt.%)	Fesil (wt.%)	FeHR/FeT	Fepy/FeHR	Hg (ppb)	Hg_corr (ppb)	Paunt (ppm)	Pdet (ppm)	Porg (ppm)	Pfe (ppm)	Preac (ppm)	Psum (ppm)	Ptot_XRF (ppm)	C/Porg (molar ratio)	C/Preac (molar ratio)
0.008	0.320	0.481	0.349	0.580	0.664	20.2	75.6	207	10.9	7.41	0.566	215	226	221	671	23.1
						16.2	61.5	211	8.6	9.45	1.93	223	231	205	358	15.2
						3.63	16.8	154	1.2	6.32	0.639	161	162	171	529	20.8
						7.72	26.4	234	10.9	10.0	0.655	245	256	246	473	19.3
						58.7	87.7	116	71.1	17.5	17.5	151	222	262	457	53.1
0.016	1.02	1.21	0.811	0.598	0.844	44.0	84.8	159	55.3	13.3	7.71	180	236	276	533	39.5
						211	276	198	100	20.5	21.1	239	340	385	2936	251
0.011	1.00	1.18	0.304	0.795	0.849	50.0	112	405	33.3	9.54	6.24	420	454	343	2408	54.7
						227	348	539	53.3	19.6	5.35	564	617	605	1788	62.2
0.015	1.36	1.50	0.419	0.781	0.904	167	287	301	62.5	16.8	1.57	319	381	452	2197	116
0.011	1.81	2.08	0.619	0.771	0.870	374	496	310	83.2	14.4	29.8	354	437	458	3827	155
0.006	1.74	1.97	0.532	0.787	0.884	251	355	543	50.1	18.3	7.63	569	619	549	3326	107
0.005	0.538	0.787		0.998	0.684	51.6	166	284	6.54	7.52	0.589	293	299	337	5999	154
0.014	1.41	1.81	0.392	0.822	0.781	52.5	80.4	548	30.8	15.8	5.75	569	600	560	4946	138
						156	212	587	83.7	12.7	24.0	624	708	729	7288	149
						14.8	105	139	0	3.93	0	143	143	164	2415	66.2
0.011	0.949	1.57	0.434	0.783	0.606	81.2	128	423	37.2	16.6	6.07	445	482	551	3551	132
						64.6	96.0	279	49.6	14.3	16.1	310	359	375	3398	157
0.013	0.936	1.49	0.511	0.744	0.630	58.6	112	246	15.3	14.5	1.47	262	277	334	1059	58.7
0.011	0.173	0.389	0.211	0.648	0.444	13.9	121	149	5.70	4.59	8.63	162	168	163	628	17.8
						7.10	92.4	134	0	2.32	1.27	138	138	182	1372	23.0
						11.7	96.3	101	0	4.05	0	105	105	121	238	9.1
						23.7	183	101	2.43	3.24	0.208	105	107	137	612	19.0
0.013	0.013	0.524	0.576	0.477	0.025	12.6	46.5	164	13.9	11.1	5.44	181	194	233	172	10.6
0.016	0.053	0.444	0.461	0.491	0.119	13.0	51.5	191	19.2	10.7	2.45	204	223	220	263	13.8
0.034	0.006	0.247	0.453	0.353	0.026	15.7	173	156	0.845	4.06	0	160	160	203	428	10.9
						23.5	291	157	0.838	4.36	1.85	163	164	196	579	15.4
0.017	0.040	0.278	0.248	0.529	0.144	13.4	153	151	1.69	3.38	0	154	156	196	1277	28.0

Table S1. Full analytical data for the analyzed samples at Nianduo (A) and Dogna (B).